

## LOW-VELOCITY IMPACT TESTS ON BASALT FIBER/ POLYPROPYLENE CORE HONEYCOMB SANDWICH COMPOSITES

**M. Bulut\***

**Keywords:** low-velocity impact, polypropylene, honeycomb, basalt fibers, failure and fracture

*The low-velocity impact behavior of polypropylene-core-based sandwich composites reinforced with basalt/epoxy facesheets was investigated by drop-weight impact tests. The impact resistance of composite samples was characterized for various impact energies according to ASTM standards. Also, the effect of facesheet thickness was explored, and the failure and fracture surfaces around the impacted region were analyzed. It was found that the thickness of facesheets played an important role in the impact properties of the honeycombs. Their residual deformation after the impact tests increased as the impact energy grew, but decreased when the number of facesheet layers increased with reducing the penetration depth and perforation.*

### 1. Introduction

Honeycomb-based sandwich structures have found broad applications in aerospace, automobile, sporting, and building construction areas, especially in the aerospace industry, due to such their properties as high energy absorption, low weight, and high mechanical (strength and stiffness) characteristics [1]. Most of such sandwich panels are made from synthetic-fiber-reinforced facesheets and cores dipped in phenolic resins, and they provide high strength/stiffness to weight ratios. However, they cannot be recycled or simply discarded when their service life expires, because of the adverse impact on the environment. Therefore, recyclable materials, like thermoplastics, are needed for producing low-cost honeycomb sandwich structures with an increased service life [2]. The impact behavior of these structures plays an important role when they are subjected to impacts by foreign objects. For this reason, to predict and prevent the impact damage of sandwich structures, their impact resistance has to be investigated [3]. Many studies have been performed on the impact behavior of fiber-reinforced composites [4-8], but

---

Mechanical Engineering Department, Faculty of Engineering, Hakkari University, Hakkari 30000, Turkey

\*Corresponding author; tel.: +90 438 2121212; e-mail: mehmetbulut@hakkari.edu.tr

---

Russian translation published in Mekhanika Kompozitnykh Materialov, Vol. 56, No. 1, pp. 177-190, January-February, 2020. Original article submitted January 15, 2019; revision submitted May 30, 2019.

less attention in this respect has been given to honeycomb sandwich structures reinforced with fiber-reinforced composites. Wu and Jiang [9] studied the crushing behavior of honeycomb sandwich composites to investigate the effect of cell dimensions, numbers, and types under quasi-static and dynamic loadings. It was found that thick cores with small cell sizes secured a higher energy absorption. Petrone et al. [10] proved that honeycomb composite structures with continuous facesheets provided a higher energy absorption, and that the presence of facesheets played an important role only for thin cores. Çalışkan and Apalak [11] conducted an experimental study on the bending response of polystyrene (PS) foam core sandwich beams reinforced by aluminum facesheets to low-velocity impacts. It was found that samples with a dense foam core revealed the lowest residual deformation in the impacted region. Rosenfeld and Gause [12] investigated the impact behavior of carbon-fiber-reinforced honeycomb sandwich structures at different impact energies. At a low impact energy, the damage occurred in the form of localized buckling, but higher impact energies initiated the formation delaminations in the reinforcing face sheets. Rhodes [13] performed a number of impact tests on sandwich structures and discovered that enhancing the crush strength of core material significantly improved the impact properties of sandwich composite structures. However, the main weakness of honeycomb structures is their poor resistance to impact loadings. During an impact event, the deformation of core with crushing reaches a critical value and increases the transverse stress, which may cause the buckling of cell wall around the impacted region [14].

Facesheet materials made of fiber-reinforced composites have been extensively used in honeycomb structures in attempt to resist the impact loadings resulting in tensile and compressive stresses due to bending effects. Various types of facesheets have been used in honeycomb structures, such as carbon, fiberglass, and natural fibers [15]. Recently, basalt fibers have preferably been used in various applications to decrease their production cost and their non-hazardous effects on the environment [16]. Basalt fiber is a natural material that melts in molten lava at 1500–1700°C and results in the formation of a volcanic rock [17]. The possibility of using basalt fibers has been examined by many researchers [18-22], and some of them have noted their superior mechanical properties compared with those of glass fibers [23-24]. In contrast to these advantages, their resistance to impact loading and damage can be considered as a weak point due to their brittle nature [25], and the number of studies related to the impact behavior of basalt-fiber-reinforced composites is very limited.

It is well known that thermoplastic materials, like polypropylene and nylon fibers, have a superior impact resistance compared with other materials, but they exhibit poor tensile, compressive, flexural, and thermal properties [26, 27]; however, it is possible to increase the impact resistance and energy absorption capacity of honeycomb-based sandwich structures by combining the low-cost polypropylene material as a core and the low-cost basalt fibers as a facesheet material to decrease production costs. Up to now, we have found no study in the literature reporting on PP-core-based honeycomb sandwich structures reinforced with basalt fibers. Therefore, in this study, the effect of facesheet thickness and impact energy on the low-velocity impact behavior of a basalt-fiber-reinforced sandwich structure with a PP honeycomb core is investigated.

## 2. Materials and Methods

### 2.1. Materials and production of test samples

A plain-weave fabric of basalt fibers with an areal density of 200 g/m<sup>2</sup>, supplied by the Spinteks Company, Turkey, was used for producing the reinforcing facesheets. As the binder, a MOMENTIVE-MGS L285 epoxy resin with a MOMENTIVE-MGS H285 hardener was employed. The facesheets were made from 2, 4, and 6 layers of the basalt fiber fabric impregnated with the epoxy resin by using the hand lay-up procedure. The mixing ratio between the epoxy and hardener was 1/0.285. The fiber fabric was impregnated with this mixture and cured for 1 h at a constant temperature of 80°C and pressure of 0.4 MPa. The production process is illustrated in Fig. 1.

The mechanical properties of the basalt/epoxy facesheets were determined experimentally using a 300-kN Shimadzu AG-X series tensile testing machine. Their average tensile strength was found to be 298.81 MPa, tensile modulus 15.59 GPa, flexural strength 236.39 MPa, and flexural modulus 14.22 GPa, but the average tensile stress–strain curve  $\sigma - \varepsilon$  is given in Fig. 2. The thicknesses of the facesheets with 2, 4, and 6 layers of the basalt fiber fabric were 0.7, 1.15, and

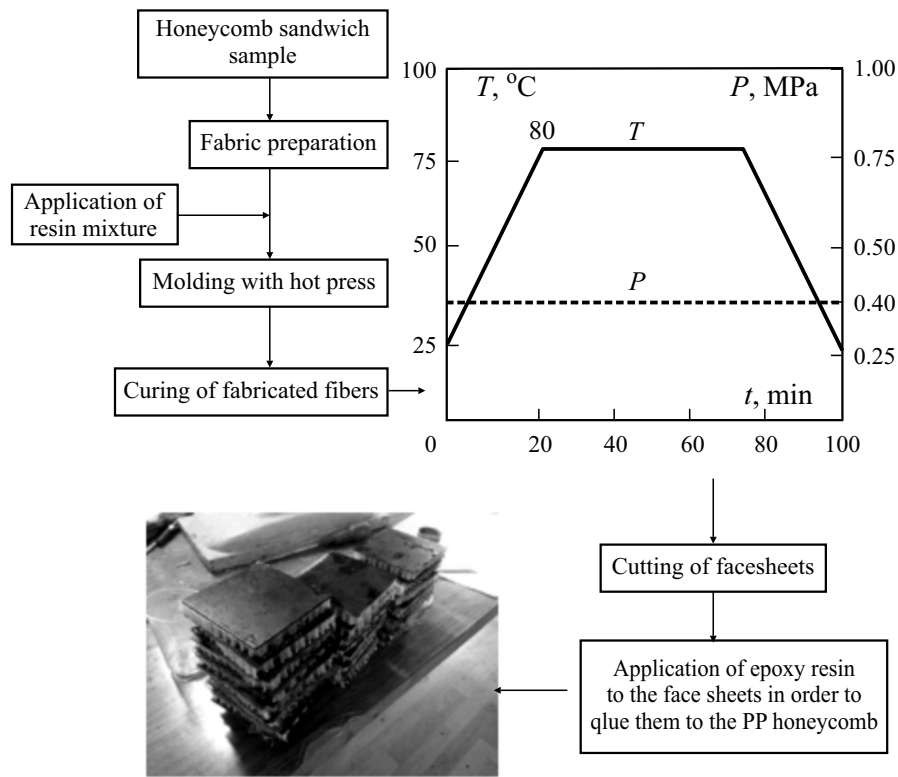


Fig. 1. Production process of test samples.

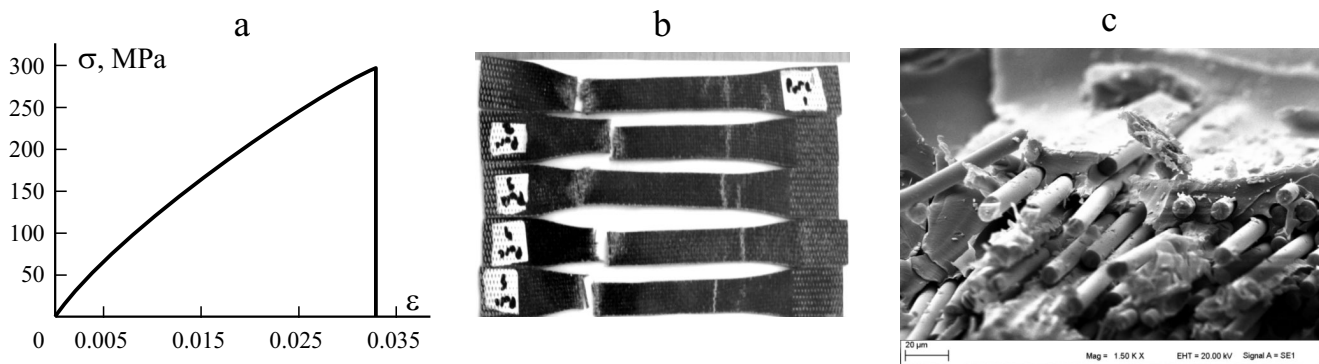


Fig. 2. Results of tensile tests on basalt/epoxy facesheets: (a) tensile stress–strain curve  $\sigma - \epsilon$  (a), fractured facesheet samples (b), and SEM image of the fractured zone (c).

1.75 mm, respectively, and their average areal density was 1488 kg/m<sup>2</sup>. A mixture of epoxy/hardener (100:40) was used to glue the basalt/epoxy facesheets to the honeycomb core. According to manufacturer's data, the density of epoxy resin was 1.18-1.2 g/cm<sup>3</sup>, flexural strength 110-120 N/mm, elastic modulus 3-3.3 kN/mm<sup>2</sup>, tensile strength 70-80 N/mm<sup>2</sup>, compressive strength 120-140 N/mm<sup>2</sup>, elongation at break 5-6.5%, and impact strength 45-55 kJ/m<sup>2</sup>. The measured thickness of the adhesive layer was 0.7 mm. The fiber volume fraction of facesheet laminates was 0.45. According to manufacturer's data, the density of the PP honeycomb was 80 kg/m<sup>3</sup>, areal density of the adhesive layer 30 g/m<sup>2</sup>, tensile strength 0.89 MPa, compressive strength 65 MPa, and shear strength 11.7 MPa.

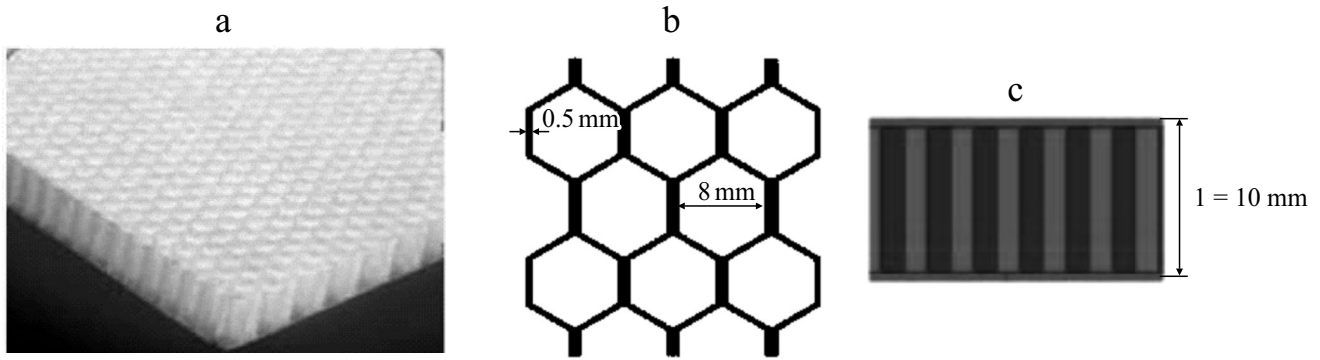


Fig. 3. PP honeycomb (a), its structure (b), and the side view (c).

The thermoplastic polypropylene honeycomb core was supplied by Dost Kimya Company, Turkey. The core had a polyester scarf with an areal density of 30 g/m<sup>2</sup> for gluing facesheets to it. The geometric characteristics of the honeycomb core structure are given in Fig. 3.

## 2.2. Impact tests of sandwich samples

A special machine, shown in Fig. 4, was used for all impact tests. It included a braking system to prevent multiple drops of impactor on test samples. The machine was equipped with two optical sensors, a flag connected to the impactor, two pneumatic pistons, a solenoid valve, and a compressor. A winch with an electromagnet was used to lift the impactor unit to the height needed.

Before impact tests, facesheets of dimensions 80×80 mm were cut from basalt/epoxy laminates and glued to the polyester scarf of PP honeycombs. Five test samples in each material group were prepared for impact tests. The diameter of the impacted circular area on the test samples was 63.75 mm. The samples were subjected to a low-velocity impact loading by a hemispherical impactor of diameter 12.7 mm. The total weight of the impactor unit was 5 kg. The effect of impact energy and facesheet thickness was studied using the drop-weight impact test procedures prescribed by ASTM D7136 standards. The histories of force action on the honeycomb structures were recorded by a piezoelectric force sensor (ICP M202B<sup>®</sup> quartz force ring) with a maximum force capacity of 44.48 kN, which was mounted just under the impactor.

All impact tests were conducted at the same conditions, and the impact energies of 10, 20, and 30 J created corresponded to the impact velocities of 2, 2.82, and 3.46 m/s, respectively. The actual velocity of impactor was evaluated by optical sensors located 25 mm above the sample surface.

## 3. Results and Discussions

Figure 5 a shows the histories  $F-t$  of force action on the test samples of sandwich composites with 2-, 4-, and 6-layer facesheets, designated as BF2L, BF4L, and BF6L at the impact energy of 10 J. As is seen, the  $F-t$  diagrams are very nonlinear, with force oscillations and different loading stages, including loadings and unloadings and two different peak loads. These oscillations are explained by vertical fiber breakages caused by the contact of impactor with the rear side of facesheets [28]. For the BF2L sample, the load jumped up again, indicating that the impactor reached the bottom layers at the impact energy of 10 J, while other samples showed only one peak load. The failure mechanisms of all test samples are illustrated in Table 1. During impacting the samples, first, the facesheet was subjected to a localized impact around the impactor, causing debonding; then, with penetration of impactor, buckling of the core material followed. BF2L samples did not withstand the impact loading at 10 J, resulting in complete penetration of facesheets at the front side, crushing of the

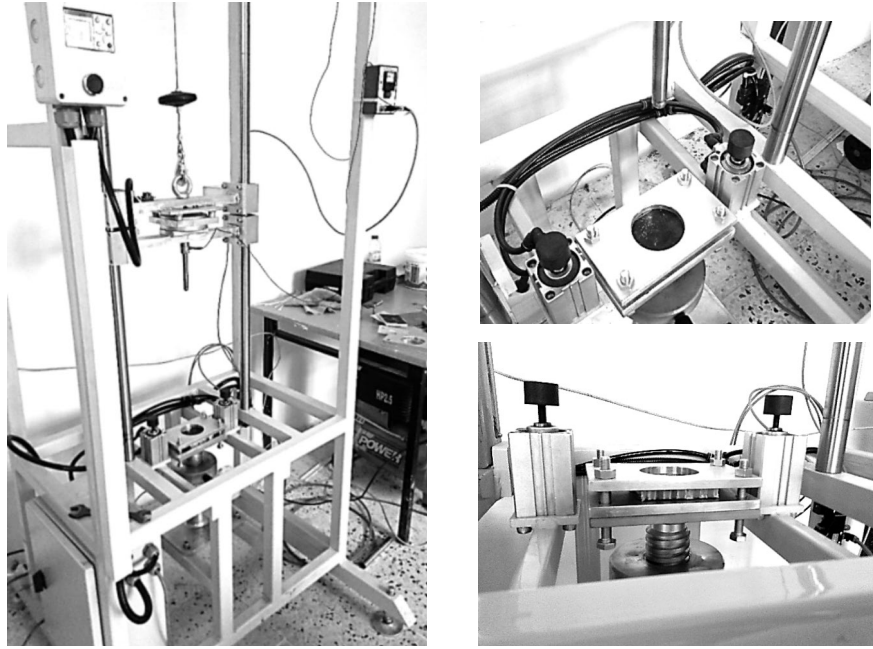


Fig. 4. Impact test machine.

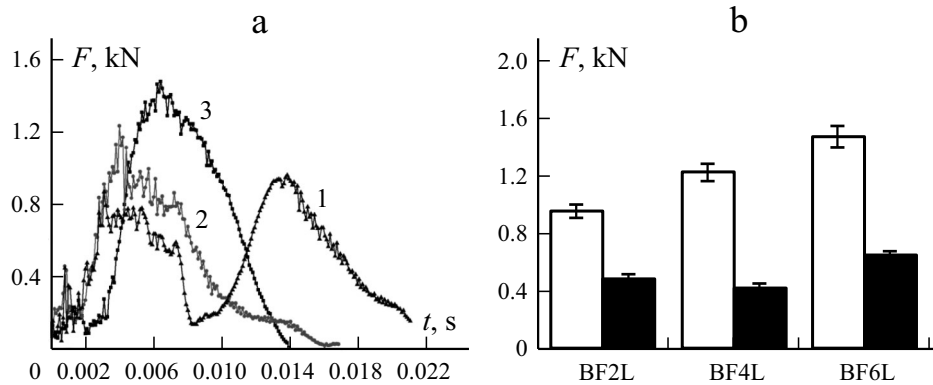


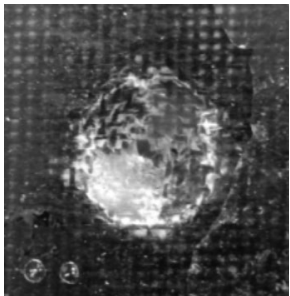
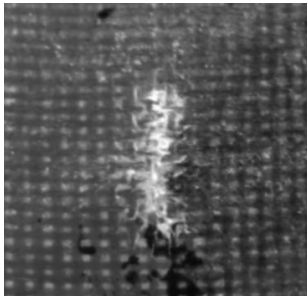
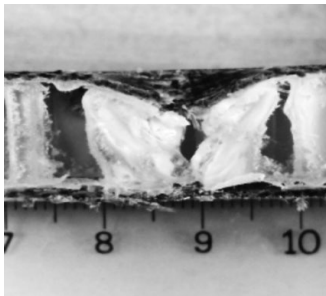
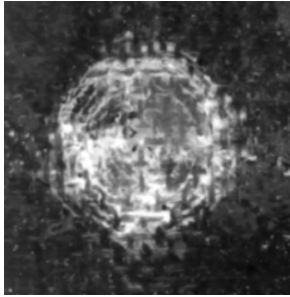
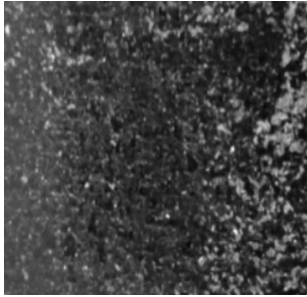
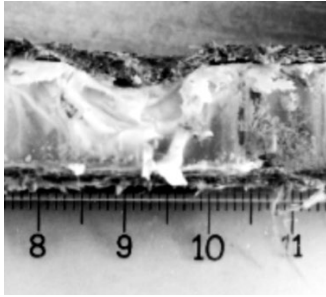
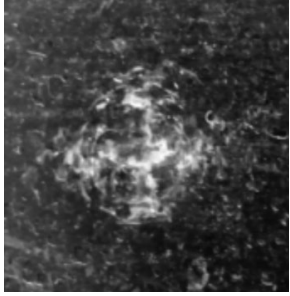
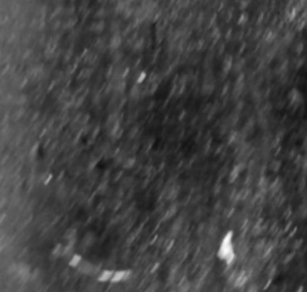
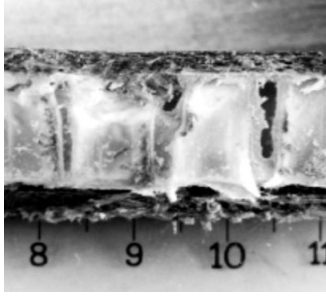
Fig. 5. Force action histories  $F-t$  at the impact energy of 10 J for the BF2L ( $-\blacktriangle-$ ), BF4L ( $-\bullet-$ ), and BF6L ( $-\blacksquare-$ ) samples (a) and the maximum ( $\square$ ) and mean ( $\blacksquare$ ) forces  $F$  (b).

core, and delaminations and fiber ruptures at the bottom layers. BF6L samples had the highest resistance to the impact loading due to their thicker facesheets, showing only a local indentation at the front side of the facesheet, without penetration and perforation. In addition, the honeycomb structure did not exhibit a high amount of buckling around the impacted cell zone. It was also found that increasing the number of facesheet layers reduced the duration of impact — it was 21, 16, and 14 ms for BF2L, BF4L, and BF6L samples, respectively.

As it is seen in Fig. 5b, the peak load increased from 0.93 for BF2L to 1.16 kN for BF4L and to 1.43 kN for BF6L with addition of two layers of basalt/epoxy facesheets, i.e., by 24.73 and 23.2%. In terms of the mean value of force, the BF6L sample showed the highest impact resistance, as seen in Fig. 5b.

The failure mechanisms of damaged samples are displayed in Table 1. Residual deformations occurred in all samples, but the residual depth decreased with increasing number of facesheet layers. The matrix cracking, fiber bending, and delamination of layers were the main damage mechanisms, but buckling was the major damage failure of the core. The shear failure

TABLE 1. Failure Mechanisms at the Impact Energy of 10 J

| Sample | Impacted side  | Rear side   | Cross-sectional view   |
|--------|--|---|--|
| BF2L   |   |   |   |
| BF4L   |   |   |   |
| BF6L   |  |  |  |

of the PP core could be clearly observed in the BF2L and BF4L samples. Fiber fractures at the bottom layers could be clearly visible in the BF2L sample, indicating the vulnerability of this honeycomb structure to impact loadings. In BF4L and BF6L samples, no damage was seen over the bottom layers, implying an increasing impact resistance at 10 J.

Figure 6a shows the loading histories of honeycomb structures at 20 J, but the failure mechanisms of the samples at 20 J are displayed in Table 2. When the impactor reached the front side of facesheets, force fluctuations increased slightly for the sample of BF2L. On increasing the facesheet thickness by addition of layers, reduction the fluctuations diminished, leading to a smooth response of transient force data. The BF2L and BF4L samples showed two different load stages (loading and unloading), implying that the impactor caused the penetration and local buckling of core structure, and reached to the bottom side of layers. Other samples (BF4L and BF6L) showed smoother curves during the loading and unloading stages, with only one peak load in the transient data. Force fluctuations were also seen clearly for the BF2L and BF4L samples, which were explained by the dynamic effect of impactor during the impact [29]. For the BF6L sample, the impactor did not reach to the bottom side of layers, pointing to its better impact properties compared with those of the other ones.

Fiber ruptures and catastrophic core crushings were visible on the impacted sides of the BF2L and BF4L samples. Full penetration at the front and bottom layers was seen only for the BF2L sample, which could be explained by the weakness of facesheets to withstand the impact loading. Although severe matrix crackings and fiber ruptures were visible at the impacted side of the BF4L sample, these types of damage at the bottom layers were insignificant, indicating only matrix damage and

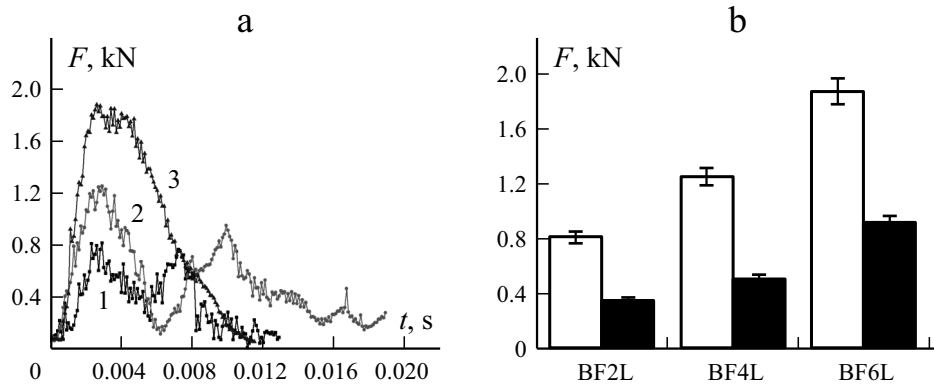
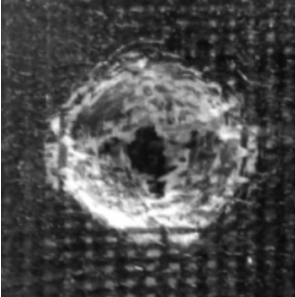
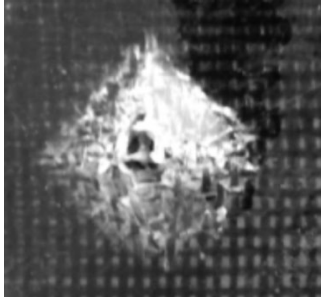
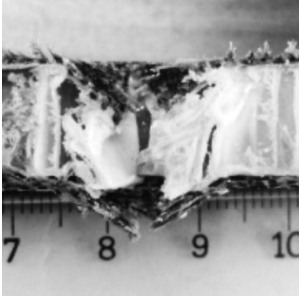
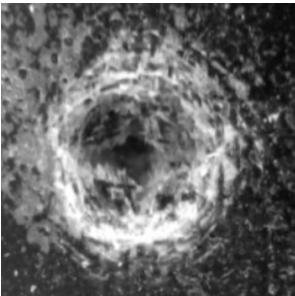
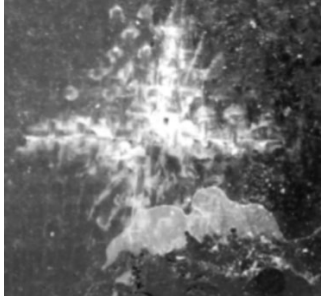
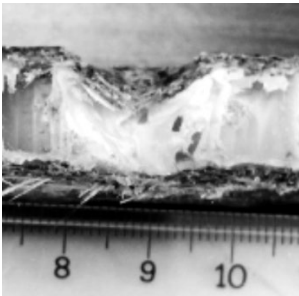
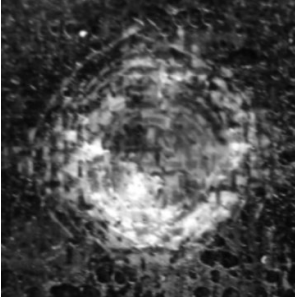
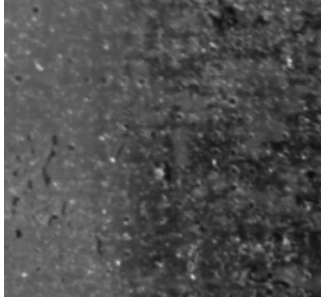
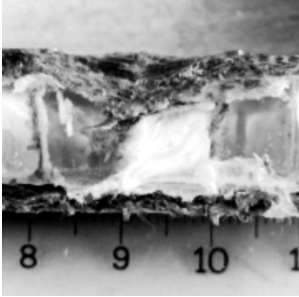


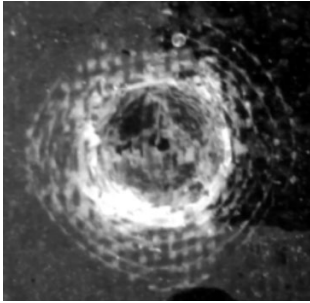
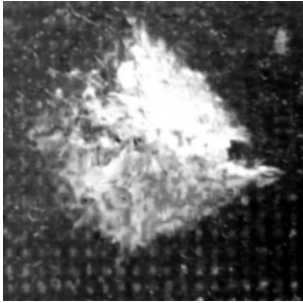
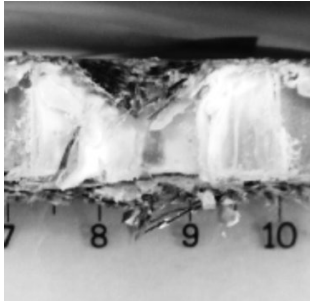
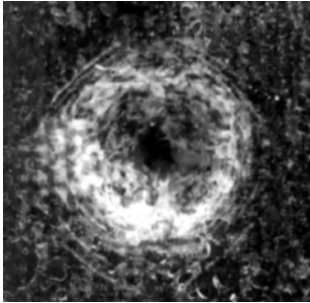
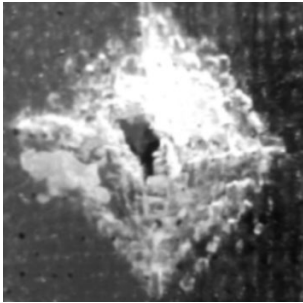
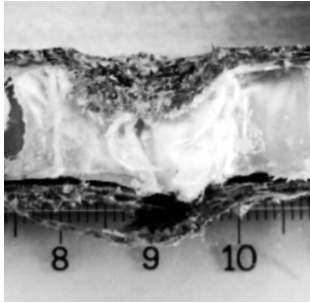
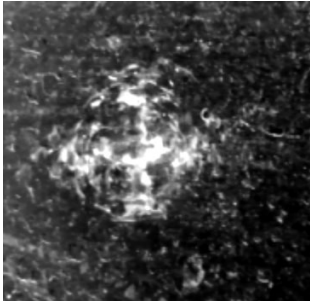
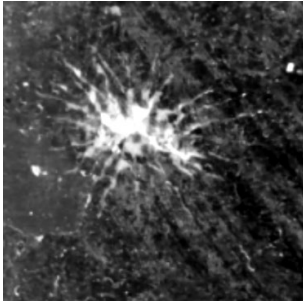
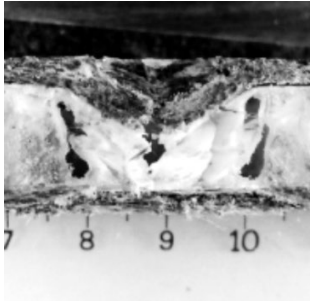
Fig. 6. Force action histories  $F-t$  at the impact energy of 20 J for the BF2L (—■—), BF4L (—●—), and BF6L (—▲—) samples (a) and the maximum (□) and mean (■) forces  $F$  (b).

TABLE 2. Failure Mechanisms at the Impact Energy of 20 J

| Sample | Impacted side   | Rear side  | Cross-sectional view  |
|--------|---|--|---|
| BF2L   |   |   |   |
| BF4L   |  |  |  |
| BF6L   |  |  |  |

delamination along the fiber direction. For the BF6L sample, only a local dent on its front surface was clearly seen, but fibers on the front side tolerated the impact loading and reduced the kinetic energy. In this stage, only one peak load was observed,

TABLE 3. Failure Mechanisms at the Impact Energy of 30 J

| Sample | Impacted side  | Rear side   | Cross-sectional view   |
|--------|--|---|--|
| BF2L   |   |   |   |
| BF4L   |   |   |   |
| BF6L   |  |  |  |

which was explained by the presence of thicker facesheets. In terms of the mean values of force data, the BF6L sample showed the highest impact resistance.

Figure 7a displays the loading histories of honeycomb structures at the impact energy of 30 J, but resulting failure mechanisms of samples are illustrated in Table 3. It is seen that all samples exhibited two different peak loads, indicating loading and unloading stages. This means that all kinetic energy of the impactor unit has been transferred to the samples, resulting in complete penetration and perforation for the BF2L and BF4L samples. Figure 7a shows that, with increasing number of facesheet layers, the fluctuations and impact duration also increased. For the BF2L sample, the load dropped during the initial loading stage due to the rupture of fibers on the impacted surfaces, but the peak force of the BF2L sample was greater than that of the BF4L sample. For the BF4L and BF6L samples, the second peak loads were lower than the first ones.

Table 3 shows the damage characteristics of samples at 30 J. The front sides of the samples were penetrated, and residual deformations arose as a result of fiber ruptures and matrix cracking. Fiber ruptures and extended delaminations between the fibers and matrix were clearly seen for the BF2L and BF4L samples. The BF2L samples were the most vulnerable honeycomb structures, exhibiting buckling in the core, and between fiber/fiber and fiber/core delaminations, and a high amount of debondings between the fibers and matrix. For the BF6L sample, only residual deformations, with buckling of core and fiber fracture on the impacted surface, occurred during the impact loading with 30 J, implying that the honeycomb structure with



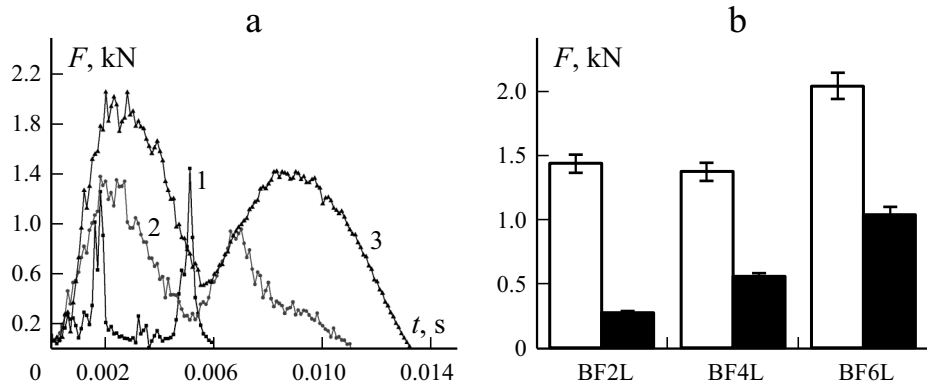


Fig. 7. Force action histories  $F-t$  at the impact energy of 30 J for the BF2L (—■—), BF4L (—●—), and BF6L (—▲—) samples (a) and the maximum (□) and mean (■) forces  $F$  (b).

this configuration had the highest strength in terms of impact loading. The impactor reached the bottom layers of facesheets, leading to matrix cracking and delamination between layers.

#### 4. Conclusion

In this study, the low-velocity impact behavior of basalt-fiber-reinforced honeycomb sandwich composites was investigated experimentally at different impact energies and facesheet thicknesses. The samples with two-layer facesheets (BF2L), did not withstand the impact energies of 10, 20, and 30 J considered, showing complete penetration of indenter. Increasing the number of layers in facesheets decreased the residual deformation and increased the peak load. The impact duration was minimum at the impact energy of 10 J. The BF6L sample showed the highest impact resistance. The addition of two layers to BF2L and BF4L increased the maximum peak load by 24.7 and 53.7%, respectively. At the impact energy of 20 J, the maximum loads increased by 53 and 129.6%, respectively, but at 30 J, — by 6.9 and 42.6%, respectively. Results of this study show that the basalt fiber, as an eco-friendly material, could be used for reinforcing sandwich composite structures with a PP honeycomb core.

#### REFERENCES

1. Y. Chen, S. Hou, K. Fu, X. Han, and L. Ye, "Low-velocity impact response of composite sandwich structures: Modeling and experiment," *Compos. Struct.*, **168**, 322–334 (2017).
2. S. Rao, K. Jayaraman, and D. Bhattacharyya, "Short fibre reinforced cores and their sandwich panels: Processing and evaluation," *Compos. Part A: App. Sci. Manuf.*, **42**, No.9, 1236-1246 (2011).
3. S. Abrate, "Impact on composite structures," Cambridge University Press, New York (1998)
4. I. Taraghi, A. Fereidoon, and F. Taheri-Behrooz, "Low-velocity impact response of woven Kevlar/epoxy laminated composites reinforced with multi-walled carbon nanotubes at ambient and low temperatures," *Mater. Des.*, **53**, 152-158 (2014).
5. F. Taheri-Behrooz, M. M. Shokrieh, and I. Yahyapour, "Effect of stacking sequence on failure mode of fiber metal laminates under low-velocity impact," *I. Iran Polym. J.*, **23**, 147–152 (2014).
6. M. Shokrieh, F. Taheri-Behrooz, H. Haftchenari, and M. Mozafari, "Size effect on the damaged areas of glass/epoxy structures under low-velocity impact," *Mech. Adv. Compos. Struct.*, **1**, No.2, 81-85 (2014).
7. V. Tita, J. de Carvalho, and D. Vandepitte, "Failure analysis of low-velocity impact on thin composite laminates: Experimental and numerical approaches," *Compos. Struct.*, **83**, 413-428 (2008).

8. S. Sánchez-Sáez, E. Barbero, and C. Navarro, "Compressive residual strength at low temperatures of composite laminates subjected to low-velocity impacts," *Compos. Struct.*, **85**, 226-232 (2008).
9. E. Wu and W.S. Jiang, "Axial crush of metallic honeycombs," *Int. J. Impact. Eng.*, **19**, 439–56 (1997).
10. G. Petrone, S. Rao, S. De Rosa, B.R. Mace, F. Franco, and D. Bhattacharyya, "Behaviour of fibre-reinforced honeycomb core under low-velocity impact loading," *Compos. Struct.*, **100**, 356–362 (2013).
11. U. Caliskan and M.K. Apalak, "Low-velocity bending impact behavior of foam core sandwich beams: Experimental," *Composites: Part B: Eng.*, **112**, 158-175 (2017).
12. K. Lauraitis, "STP723-EB fatigue of fibrous composite materials," West Conshohocken, PA: ASTM International (1981). <https://doi.org/10.1520/STP723-EB>
13. M. D. Rhodes, "Impact fracture of composite sandwich structures," *Proc ASME/AIAA/SAE, 16th Struct., Struct. Dyn. Mater. Conf.*, 311–316 (1975).
14. O. Balcı, O. Çoban, M.Ö. Bora, E. Akagündüz, and E.B. Yalçın, "Experimental investigation of single and repeated impacts for repaired honeycomb sandwich structures," *Mater. Sci. Eng. A*, **682**, 23-30 (2017).
15. A. McCracken and P. Sadeghian, "Partial-composite behavior of sandwich beams composed of fiberglass facesheets and woven fabric core," *Thin-Walled Struct.*, **131**, (805-815) 2018.
16. J. Sim, C. Park, and D. Y. Moon, "Characteristics of basalt fibre as a strengthening material for concrete structures," *Compos Part B: Eng.*, **36**, 504-512 (2005).
17. M. Bulut, "Mechanical characterization of basalt/epoxy composite laminates containing graphene nanopellets," *Compos B: Eng.*, **122**, 71-78 (2017).
18. V. Lopresto, C. Leone, and D.I. Iorio, "Mechanical characterisation of basalt fibre reinforced plastic," *Compos. B: Eng.*, **42**, 717–23 (2011).
19. T. Czigany, "Special manufacturing and characteristics of basalt fiber-reinforced hybrid polypropylene composites: mechanical properties and acoustic emission study," *Compos. Sci. Technol.*, **66**, No.16, 3210-3220 (2006).
20. Q. Liu, H.S. Giffard, M.T. Shaw, A.M. McDonnell, and R.S. Parnas, "Preliminary investigation of basalt fiber composite properties for applications in transportation. The official newsletter of the international institute for FRP in construction," **2**, 6–8 (2005).
21. M. T. Kim, M. H. Kim, K. Y. Rhee, and S.J. Park, "Study on an oxygen plasma treatment of a basalt fiber and its effect on the interlaminar fracture property of basalt/epoxy woven composites," *Compos. B: Eng.*, **42**, 499–504 (2011).
22. T. Deák, T. Czigány, P. Tamás, and C.S. Németh, "Enhancement of interfacial properties of basalt fiber-reinforced nylon 6 matrix composites with silane coupling agents," *Exp. Polym. Lett.*, **4**, 590–598. (2010).
23. J.S. Szabo and T. Czigany, "Static fracture and failure behavior of aligned discontinuous mineral fiber-reinforced polypropylene composites," *Polym. Test.*, **22**, 711–719 (2003).
24. Q. Liu, M. T. Shaw, A. M. McDonnell, and R. S. Parnas, "Investigation of basalt fiber composites mechanical properties for application in transportation," *Polym. Compos.*, **27**, 41–48 (2006).
25. X. Wang, "Low-velocity impact properties of 3D woven basalt/aramid hybrid composites" *Compos. Sci. Technol.*, **68**, 444–450 (2008).
26. M. T. Dehkordi, H. Nosraty, M. M. Shokrieh, G. Minak, and D. Ghelli, "Low-velocity impact properties of intraply hybrid composites based on basalt and nylon woven fabrics," *Mater. Des.*, **31**, 3835–3844 (2010).
27. J. E. McIntyre, *Synthetic fibers: nylon, polyester, acrylic, polyolefin*. Woodhead Publishing, CRC Press. Boca Raton-Boston-Newyork-Washington, DC-Cambridge-England (2005)
28. M. V. Hosur, M. Abdullah, and S. Jeelani, "Manufacturing and low-velocity impact characterization of hollow integrated core sandwich composites with hybrid face sheets," *Compos. Struct.*, **65**, 103-115 (2004).
29. G. B. Chai and P. Manikandan, "Low-velocity impact response of fibre-metal laminates – A review," *Compos. Struct.*, **107**, 363-381 (2014)